A SIMPLE MODEL OF SNOW SLOPE STABILITY DURING STORMS

P. Hayes [a], C. Wilbour [b], R. Gibson [b], H.P. Marshall [c] and H. Conway [a]

[a] Earth and Space Sciences, University of Washington, Box 351310, Seattle, WA 98195, USA

[b] Washington State Department of Transportation, Box 1008, Snoqualmie Pass, WA 98068, USA

[c] Institute of Arctic and Alpine Research, University of Colorado, Box 450, Boulder, CO 80309, USA

ABSTRACT: Snow slope stability is controlled by the geometry of the start zone and the mechanical properties of the snow pack. Here we report progress toward developing a simplified model of the evolution of snow slope stability during storms. The model (SNOSS) keeps track of the evolving gravitational stress imposed by the new snow and the strength of sub-surface layers. Avalanching is predicted when the down-slope component of the gravitational shear stress from the overburden exceeds the resisting basal strength of a buried weak layer; there is a competition between the rate of loading from new snow and the rate of strengthening of buried layers. In theory, SNOSS should provide a conservative estimate (predicting failure earlier than expected) because it does not account for influences such as longitudinal stress gradients in the slab, or non-linear or time-dependent properties of snow. Much of the appeal of SNOSS is that it is physically based (with empirical parameterizations) and its input requirements are easily measured and often readily available. The model runs on a PC and can be used operationally to track the evolving stability. The model is tested using hourly measurements of precipitation and temperature from a network of weather stations and observations of avalanche occurrence near Snoqualmie Pass in the Washington Cascades during the winter of 2003-04.

Keywords: snow slope stability, avalanches, modeling

1. INTRODUCTION

Dry snow slab avalanches are controlled by the mechanical properties of the snow-pack and the geometry of the start zone. Slab avalanches initiate when a relatively cohesive slab of snow overlies an extensive weak layer, with failure occurring when the overburden stresses exceed the shear strength of the basal layer. There is a strong motivation to predict snow slope stability because forecasting slab avalanches is difficult; however, since fully physical three-dimensional models require details of the thermal and mechanical conditions in snow slabs which are not regularly measured and are often unknown and not well understood, simplifying assumptions are necessary for operational applications. Early models of snow slope stability examined the balance between longitudinal and lateral stresses in a slab increasing to compensate for the loss of basal shear support, with failure occurring when the stresses exceeded the strength (Perla and LaChapelle, 1970; Brown et al, 1972; Perla, 1980). Slip weakening models of avalanche initiation (McClung, 1979; 1981; Gubler and Bader, 1989; Bader and Salm, 1990) were inspired by experimental results (McClung, 1977) that showed that snow may strain-soften under conditions of rapid shearing.

Recent advances in electronics and telemetry now make it possible to transmit meteorological data from remote weather stations in real-time. Here we use hourly measurements of temperature and precipitation from a network of weather stations near Snoqualmie Pass in the Washington Cascades for model input. Snoqualmie Pass, elevation 900 m with surrounding terrain to 1700 m, experiences a maritime climate with winter storms depositing up to 1 m of new snow. Direct action avalanches are common, and often have a major impact on winter travelers and commerce traversing Interstate 90, the major highway crossing the Cascades from Puget Sound. Success is judged by comparing the modeled time of failure with observations of avalanche activity.

2. CONCEPTUAL MODEL

Using an infinite-slope approximation, and neglecting longitudinal forces, snow slope stability is estimated from a balance of forces; with slab failure predicted when the down-slope component of the shear stress imposed by the overburden exceeds the shear strength of a buried weak layer (Fig. 1) (Endo, 1991; Conway and Wilbour, 1999, Conway and Carran, 2004). Hourly measurements of temperature and precipitation are used to

calculate components of shear stress and strength.

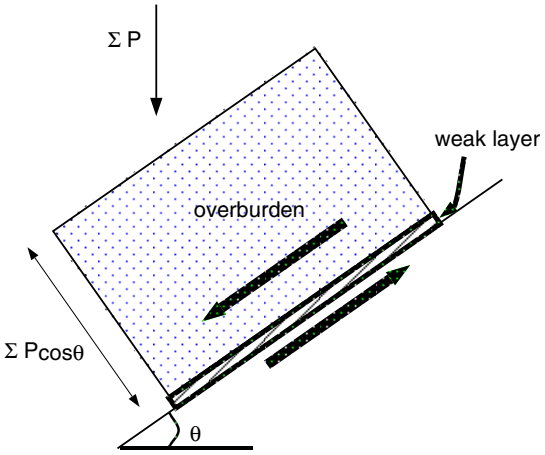

Figure 1: Neglecting longitudinal forces, slope failure is expected when the shear stress from the overburden exceeds the shear strength of a buried weak layer.

2.1 Evolution of basal shear stress

The down-slope component of the shear stress on a planar slab inclined at angle ϑ after time t is:

$$\sigma_{xz}(t) = g\cos\vartheta\sin\vartheta\sum_0^t P \qquad (1)$$

Where the gravitational constant g = 9.8 m s^{-2} and $\sum_0^t P$ is the cumulative precipitation in kg/m^2.

2.2 Evolution of basal shear strength

The mechanical properties of snow depend strongly on microstructure; however, these properties are often not known or measured. Because bulk density is easily and often measured, the shear strength of a buried weak layer is assumed to be a function of density. Following Gibson and Ashby (1987), the (elastic) shear strength of a basal layer is calculated from:

$$\sigma_f(t) = A_1\rho^2 \qquad (2)$$

where ρ is snow density at time t and A_1, which includes a shape factor dependant on snow crystal type, is based on measurements (Perla et al, 1982; Jamieson and Johnston, 1999).

Density is taken from measurements if available. Where the density of the basal layer is not known, the density of new snow is estimated from:

$$\rho(0) = A_2\varepsilon_{sat} \qquad (3)$$

where the scaling factor A_2 was derived empirically using measurements of LaChapelle (1969) and ε_{sat} is the saturation vapor pressure over water.

The initial snow density, and associated shear strength of the basal layer vary strongly with temperature since ε_{sat} varies strongly with temperature.

The density of snow on the ground increases with compaction by the overburden stress σ_{zz} and because of metamorphic processes, which are modeled as an effective stress σ_m. A viscous densification model is used to track the evolution of the density of buried layers:

$$\frac{d\rho}{dt} = \rho\times\frac{\sigma_m + \sigma_{zz}}{\eta_{zz}} \qquad (4)$$

where η_{zz}, the compactive viscosity, is:

$$\eta_{zz} = C * \exp\left(\frac{E}{R * T_s}\right) * \rho^4 \qquad (5)$$

T_s is the temperature of the basal layer, which is taken as the air temperature at the time of deposition.

We modified Abe's (2001) viscosity model by fitting an Arhenius relationship to the 4 data points Abe's model was derived from.

$$\sigma_{zz}(t) = g\cos^2\theta\sum_0^t P \qquad (6)$$

and $\sigma_m(t) = 75$, which is the average found from compaction measurements near the surface where $\sigma_{zz}(t) \approx 0$ (Marshall et al, 1999). In reality,

$\sigma_m(t)$ is expected to range from being positive (equilibrium metamorphism) to negative under large temperature gradients (kinetic growth metamorphism).

2.3 Stability index and time to failure

The average stability index $\overline{\sum_z}(t)$ at depth z and time t is:

$$\overline{\sum_z}(t) = \frac{\sigma_{fz}(t)}{\sigma_{xz}(t)} \quad (7)$$

Where $\sigma_{xz}(t)$ comes from Eq. (1). We solve for $\rho_z(t)$ iteratively (Eqs. (4) and (5)) and use these in Eq. (2) to calculate $\sigma_{fz}(t)$.

The expected time to failure $t_f(t)$ at time t is:

$$t_f(t) = \frac{\overline{\sum_z}(t)(-1.0)}{d\overline{\sum_z}(t)/dt} \quad (8)$$

$t_f(t)$ contains information about both the magnitude and the current trend in $\overline{\sum_z}(t)$.

3. CASE HISTORIES

New snow density measurements and precipitation and air temperature observations from the Snoqualmie Pass area in the Washington Cascades are used to run the model for eight avalanche cycles from the 2003-04 winter. New snow density, which is measured daily at the Department of Transportation (DOT) study plot (915 m), is used to calculate the initial strength of new snow (Eq. 2) if the measured density is representative of the expected basal layer density. Otherwise, the mean air temperature from the study plot and a nearby ridge top (1160 m) is used to calculate the initial basal layer snow density (Eq. 3), assuming that the snow temperature is the same as the air temperature at the time of deposition. This approximation is reasonable during short periods of snowfall; however, it is invalid during periods of rapid warming or rain when heat may quickly enter the snowpack. Hourly measurements of precipitation from a heated gauge at the local study plot are used to calculate the evolution of shear stress $\sigma_{xz}(t)$ (Eq. 1) and strength $\sigma_f(t)$ (Eq. 2) for slopes of 35-40°. Alternatively, air temperature and precipitation gauge measurements from a nearby ski area could be used. Model results from two of the avalanche cycles are presented in detail, with a summary of the remaining six cycles included in section 4.

3.1 January 6-7, 2004 (Day 6, 7)

A very cold period in early January 2004 led up to the one large avalanche cycle of the 2003-04 winter, with avalanche control producing significant results late on January 6th and again on the 7th and with widespread natural soft slab avalanches during the late afternoon and early evening on January 7th. Following a few days at the beginning of the month with relatively light amounts of new snow, air temperatures decreased significantly and snowfall ended early January 4th. It remained dry through early morning January 6th, and air temperatures remained unusually cold, ranging from ≈ -15° C to -21° C from late on the 4th through the 6th. 5-7 mm surface hoar developed in the DOT study plot during this cold dry period with larger surface hoar noted in other locations. Avalanche personnel observed "squaring" from kinetic growth metamorphism.

Snowfall started at 6am on the 6th, and it is this layer, or the existing surface hoar, that likely became the basal layer for subsequent avalanches. By 1700 on the 6th, with 10mm water equivalent (w.e.) recorded, the DOT did control on paths east of the Cascade crest. It was dark, so the full extent of the resulting slides was unknown; however, debris crossed the two highway lanes not covered by the East Snow Shed. Reports indicate that this was the largest slide from the least amount of 24 hour snow in memory. At 0345 on January 7th, blowing snow resulted in a full pass closure for zero visibility. The DOT took advantage of this closure to do avalanche control work in several paths at 0700. The shots produced widespread sympathetic activity with one slide filling a catchment ditch and hitting the highway. Control work in paths east of the Cascade crest at 1100 and later in paths west of the crest also yielded substantial results with the most impressive avalanches initiated by a tram that simultaneously released 3-4 separate 26-pound shots. According to eye witnesses, "The results were spectacular. Every snow grain that could

move did." One of the slides jumped a very large catchment dam. At 1645 and continuing through late in the evening, a widespread natural avalanche cycle occurred everywhere west of the crest that had not been shot.

Figure 2a shows the cumulative precipitation from the onset at 6 am on the 6th (day 6.25) through the natural avalanche cycle on the 7th with total precipitation ≈ 50 mm. During this same period, air temperatures rose to -10° C at pass level. Figure 2b shows the modeled strength of the basal layer and stress from the overburden for start zones of 35°. Figure 2c shows the stability index (the ratio of strength to stress) with failure predicted when the stability index is less than 1, which occurred by 1800 on January 7th (day 7.75). Figure 2d, which shows the time to failure, also indicates failure by 1800. For steeper slope angles, failure is predicted at earlier times (failure at 1200 for a 45° slope). Although control work produced significant avalanching late on the 6th and again on the 7th, (the explosives used produced sufficient stress to exceed the strength of the basal layer), Figs 2b, 2c,and 2d all indicate that modeled basal layer strength significantly exceeded the overburden stress until mid-morning on the 7th independent of slope angle. Given the sensitivity of the overburden stress to slope angle and the sensitivity of the basal layer strength to initial snow density (temperature), the sharply decreasing trend of the stability index as it approaches 1.0 is a more important tool for avalanche practitioners than is relying on the precise time of failure indicated by the model.

3.2 January 25-26, 2004 (Days 25, 26)

An avalanche cycle on January 25-26 involved temperature fluctuations near freezing. Although 9.5 inches of new snow was recorded in the DOT study plot on the 25th, only a few sluffs from ski cutting were reported. However, as precipitation turned to rain on the 26th, avalanche control produced moderate results and a natural avalanche cycle occurred west of the crest. We present this case as an example of SNOSS predicting relatively stable conditions; however, it also demonstrates some of the limitations of SNOSS.

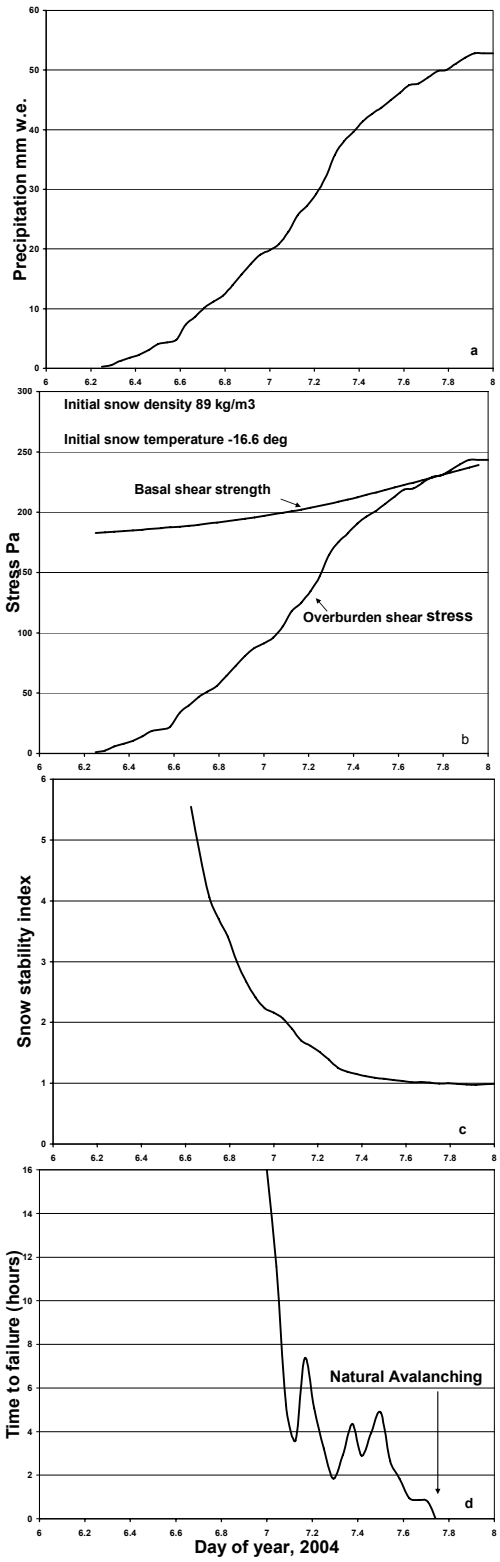

Fig.2 Measurements of cumulative precipitation at 915 m starting at 0600 hr on January 6, 2004 (day 6.25) (a). Also shown is the strength of the basal layer and shear stress from the overburden for a 35 deg slope (b), the average stability index at the basal layer (c), and the expected time to failure (d).

Freezing rain on January 23rd turned to snow on the 24th. Figure 3a shows cumulative precipitation in mm water equivalent starting with the transition from freezing rain to snow at 6 am on the 24th. With 24 cm of new snow reported by early on the 25th, ski cutting at Alpental, the neighboring ski area, produced only loose sluffs. Wet snow, which fell through the 25th, turned to rain by late morning on the 26th. The evolution of the strength of the basal layer and stress from the overburden are shown in Figure 3b. Although the overburden stress for this case eventually exceeds the stress at failure for the January 7th avalanche cycle (~250 Pa), the initial basal layer strength (~350 Pa) and rate of densification are so high (as a result of near freezing temperatures) that stress remains significantly less than strength. The snow stability index, shown in Figure 3c, decreases rapidly initially, then levels out through early on the 25th when it again decreases. The time of the decrease in stability index on the 25th correlates with the loose sluffs produced at Alpental. With temperatures below freezing on the 25th, SNOSS adequately models stress and strength.

Heavier precipitation on the 26th produced steadily increasing overburden stress; however, modeled basal layer strength was so high that unrealistic precipitation rates would be required for modeled stress to exceed strength. As temperatures rose above freezing on the 26th, and snow turned to rain, DOT avalanche control produced moderate results in paths near the East Shed, and a natural avalanche cycle occurred west of the pass. The onset of rain often produces abrupt changes in stability with associated rapid and widespread avalanching (Conway, 1998). With the physics associated with rain on snow not well understood and beyond the current scope of SNOSS, it is not surprising that the model indicates stable conditions, whereas the onset of rain resulted in avalanching at Snoqualmie Pass.

4. DISCUSSION

At Snoqualmie Pass, the 2003-04 winter produced one large avalanche cycle (January 6-7, 2004) and a moderate rain on snow cycle (Janaury 25-26, 2004). Snoss predicted stability for 6 additional avalanche cycles. Two of these cycles involved rain on snow, with minimal results from control and small natural wet loose avalanches observed. A 3-day avalanche cycle, which occurred with near but below freezing temperatures and no rain, resulted in small avalanches, both natural and from control. The three remaining avalanche cycles, which all occurred with relatively light amounts of new snow and cooler temperatures, also produced minimal results. SNOSS predicted stability during each of these cycles because initial basal layer strength was high or because the rate of loading was light and did not exceed the rate of strengthening.

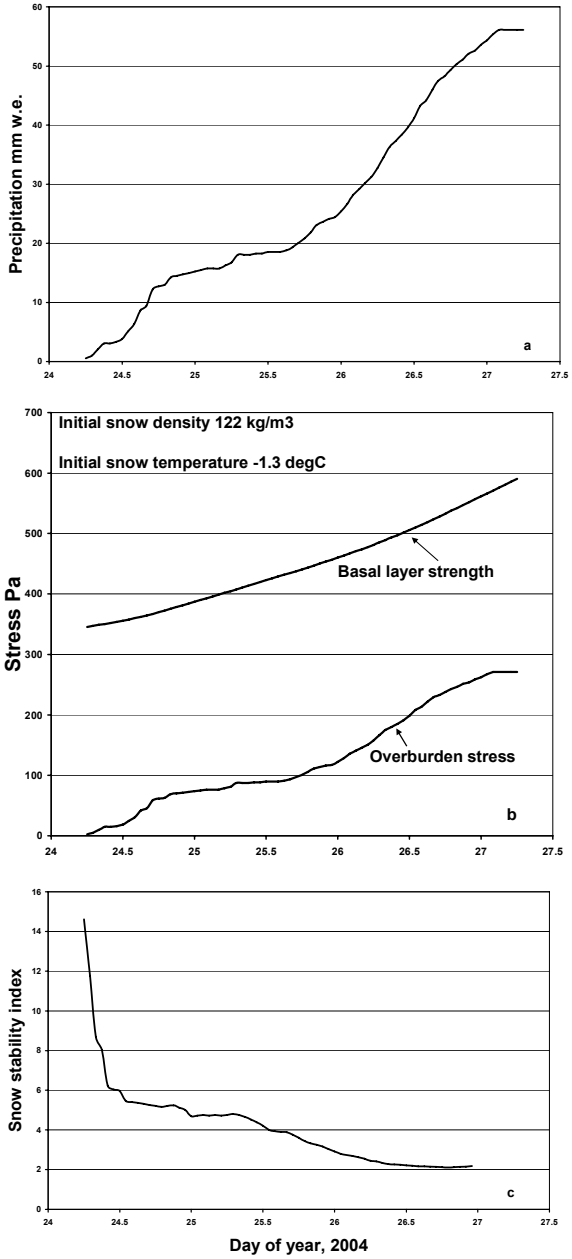

Fig.3. Measurements of cumulative precipitation at 915 m starting at 0600 hr on January 24, 2004 (day 24.25) (a). Also shown is the strength of the basal layer and shear stress from the overburden for a 40 deg slope (b), the average stability index at the basal layer (c), and the expected time to failure (d).

SNOSS's predictions of slab failure (overburden stress exceeds basal layer strength) are sensitive to temperature and precipitation rate. In the absence of basal layer density measurements, air temperature is used to estimate the initial basal layer snow density (Eq. 3) and the evolution of basal layer strength (Eq. 2). The initial basal layer strength, with density computed from temperature, increases from 150 Pa at -7° C to 326 Pa at -1° C (Table 1). After 72 hours, the basal layer strengths are 459 Pa and 739 Pa at -7° and -1° C respectively. Table 1 also gives the minimum hourly precipitation rates that are required to initiate slab failure on 40° slopes within 3 days of the onset of precipitation for a series of temperatures that are typical of precipitation events at Snoqualmie Pass. The precipitation rates are in 0.25 mm increments, which is the resolution of the gauge measurements. At -1° C, a constant hourly precipitation rate of 2.5 mm w.e. is required for failure in 70 hours, with stable conditions predicted for precipitation rates less than 2.5 mm w.e.. At -7° C, an hourly precipitation rate of 1.5 mm w.e. results in failure in 46 hours. These results indicate that for slab failure to be predicted, the basal layer must be deposited at cold temperatures, or the precipitation rate must be consistently high.

Table 1. Minimum hourly precipitation rates required to initiate slab failure on 40° slopes within 3 days of the onset of precipitation.

Snow Temperature °C	$\sigma_f(0,72)$ (Pa)	Precipitation Rate (mm/hr)	Failure (hrs)
-1	362 / 739	2.5	46
-3	271 / 638	2.3	39
-5	202 / 555	2.0	50
-7	150 / 459	1.5	70

$\sigma_f(0,72)$ is the basal layer strength at deposition (0) and after 72 hours.

Temperature and precipitation measurements that may not accurately represent conditions in avalanche start zones, and inaccuracies in the measurements themselves, introduce errors in model results. Differences in elevation, topography, and winds cause snow depths in start zones to differ from those in valley bottoms, where most measurements are taken (Fohn and Meister, 1983; Schmidt et al, 1984; Gauer, 1998). In complex terrain, precipitation may vary strongly over short distances. For example, Sinclair et al (1997) document 24-h precipitation measurements of 125 and 315 mm at gauges 2 km apart in New Zealand. In addition, precipitation measurement is afflicted by many error sources, especially at low temperature. Gauge catch decreases with increasing wind speed, resulting in an undercatch of up to 50% or more for snowfall (Groisman and Legates, 1994; Yang et al, 1998).

5. CONCLUSIONS

SNOSS is appealing as a tool for operational forecasting of direct action avalanches because it is physically based and has few empirical parameters. SNOSS runs on a PC and its input requirements, new snow density, temperature and precipitation measurements, are readily available and regularly measured. Quantitative precipitation forecasts may be used as model input for avalanche forecasting; however, if forecast precipitation is used, practitioners must monitor measured precipitation, as forecast quantities are often incorrect. The trend of the stability index (strength/stress) is a more important tool for avalanche practitioners than is relying on the precise value of the stability index or the predicted time of failure because the model is sensitive to temperature and precipitation rate, measurements of which may be afflicted by errors and may not be representative of conditions in avalanche start zones.

6. ACKNOWLEDGEMENTS

This work was supported and funded by the U.S. National Science Foundation and Washington State Department of Transportation.

7. REFERENCES

Abe, O., 2001. Creep experiments and numerical simulations of very light artificial snowpacks. Annals Glaciol, 32, 39-43.

Bader, H. -P. and B. Salm, 1990. On the mechanics of snow slab release. Cold Reg. Sci. and Tech., 17, 287-300.

Brown, C. B., R. J. Evans, and E. R. LaChapelle, 1972. Slab avalanching and the state of stress in fallen snow. J. Geophys. Res. 77(24), 4570-4580.

Conway, H., 1998. The impact of surface perturbations on snow-slope stability. Ann. Glaciol. 26, 307-312.

Conway, H., and W. Carran, 2004. Forecasting direct-action avalanches during storms. In

Proceedings, International Symposium on Snow Monitoring and Avalanches, 12-16 April, 2004, Manali, India. 37-46.
Conway, H. and C. Wilbour, 1999. Evolution of snow slope stability during storms. Cold. Reg. Sci. and Tech., 30 (1-3), 67-77.
Endo, Y., 1991. Time variation of stability index in new snow on slopes. Proc. Japan- u.s. Workshop on Snow Avalanche, Landslide, Debris Flow Prediction and Control, 85-94.
Fohn, P. and R. Meister, 1983. Distribution of snow drifts on ridge slopes: measurements and theoretical approximations. Ann. Glaciol., 4, 52-57.
Gauer, P., 1998. Blowing and drifting snow in Alpine terrain: numerical simulation and related field measurements. Ann. Glaciol., 26, 174-178.
Gibson, L. J. and M. F. Ashby, 1987. Cellular solids: structure and properties. Solid State Sciences Series. Cambridge University Press, Cambridge, 510 pp.
Groisman, P. V. and D. R. Legates, 1994. The accuracy of United States precipitation data. Bull. Amer. Meteor. Soc., 75, 215-227.
Gubler, H. and H.-P. Bader, 1989. A model of initial failure of slab-avalanche release. Annals Glaciol., 13, 90-95.
Jamieson, J. B. and C. D. Johnston, 1999. Snowpack factors associated with strength changes of buries surface hoar layers. Cold Reg. Sci. and Tech., 30 (1-3), 19-34.
LaChapelle, E. R., 1969. Properties of snow. Paper prepared for Hydrologic Systems course presented by College of Forest Resources, University of Washington, Seattle, 21 pp.
Marshall, H.-P., H. Conway and L. A. Rasmusson, 1999. Snow densification during rain. Cold Reg. Sci. and Tech., 30 (1-3), 35-40.
McClung, D. M., 1977. Direct simple shear tests on snow and their relation to slab avalanche formation. J. Glaciol., 19(81), 101-109.
McClung, D. M., 1979. Shear fracture precipitated by strain-softening as a mechanism of dry slab release. J. Geophys. Res. 84(87), 3519-3526.
McClung, D. M., 1981. Fracture mechanical models of dry slab avalanche release. J. Geophys. Res. 86(B11), 10783-10790.
Perla, R., 1980. Avalanche release, motion and impact. In Dynamics of Snow and Ice Masses (Ed. S. C. Colbeck). Academic Press, pp 397-468.
Perla, R., T. M. Beck and T. T. Cheng, 1982. The shear strength index of alpine snow. Cold Reg. Sci. and Tech., 6(1), 11-20.
Perla, R. and E. R. LaChapelle, 1970. A theory of snow slab failure. J. Geophys. Res. 75(36), 7619-7627.
Schmidt, R. A., R. Meister, H. Gubler, 1984. Comparison of snow drifting measurements on an alpine ridge crest. Cold Reg. Sci. and Tech., 9(2), 131-141.
Sinclair, M. R., D. S. Wratt, R. D. Henderson, and W. R. Gray, 1997. Factors affecting the distribution and spillover of precipitation in the Southern Alps of New Zealand – A case study. J. Appl. Meteor., 36, 428-442.
Yang, D., B. E. Goodison, J. R. Metcalfe, V. S. Golubev, R. Bates, T. Pangburn, C. L. Hanson, 1998. Accuracy of NWS 8-inch standard nonrecording precipitation gauge: results and application of WMO intercomparison. J. Atmos. Ocean Technol., 15(1), 54-68.